
The manuscript is a preprint and has been submitted for publication in GRL. Please note that, the manuscript has not undergone peer review. Subsequent versions of this manuscript may have slightly different content. If accepted, the final version of this manuscript will be available via the 'Peer-reviewed Publication DOI' link on the right-hand side of this webpage. Please feel free to contact any of the authors. We welcome feedback!

1 **Variations in Earth's 1D viscosity structure in different**
2 **tectonic regimes**

3 **Anthony Osei Tutu and Christopher Harig**

4 Department of Geosciences, University of Arizona, Tucson, Arizona, USA

5 **Key Points:**

- 6 • Distinct regional 1D viscosity structures of the Pacific and Atlantic tectonic man-
7 tles
8 • Subducted oceanic crust with slabs affect strong viscosity interface in the tran-
9 sition zone
10 • Slabs dehydration from ancient subduction in the Atlantic mantle suggests low
11 viscosity upper mantle

Abstract

Past estimates of Earth’s mantle viscosity profile using the long-wavelength geoid suggest an increase in viscosity from the upper to lower mantle of roughly 2-3 orders of magnitude. We use a spatio-spectral localization technique with the geoid to estimate a series of locally constrained viscosity profiles covering two unique regions, the Pacific and Atlantic hemispheres. The Pacific region exhibits the conventional Earth’s 1D rheology with a factor of roughly 80-100 increase in viscosity occurring at transition zone depths. The Atlantic region in contrast does not show significant viscosity jumps with depth, and instead has a near uniform viscosity in the top 1000 km. Our inferred viscosity variations between the two regions could be due to the prevalence of present-day subduction in the Pacific region and the relative infrequency of slabs in the Atlantic, combined with a possible hydrated transition zone and mid-mantle in the Atlantic region by ancient subduction.

Plain Language Summary

The surface and internal structures of Earth move on a time scale of tens to hundreds of million years. The slow motion of continents as shown by satellite observations is dependent on the viscosity of Earth’s interior. We use mathematical methods and computer simulations to study viscosity/strength as a function of depth in two regions: the Pacific and Atlantic hemispheres. Our calculations show that the Pacific region of Earth’s interior is relatively stronger than the Atlantic region. We interpret these differences as the results of the spatial distribution of subduction, where oceanic lithosphere is recycled into mantle.

1 Introduction

The viscosity of Earth’s mantle is fundamental to the operation of convection and plate tectonics, and as a result, it has been extensively studied over the past several decades. Many studies have used the long wavelength ($l = 2-3$) geoid and mantle flow calculations to explore the radial viscosity and density structures of the mantle (Hager, 1984; M. A. Richards & Hager, 1984; Forte et al., 1994; Panasyuk & Hager, 2000; Steinberger & Calderwood, 2006; Forte et al., 2013). Hager and Richards et al. (Hager & Richards, 1989) showed that about 90% of the observed long-wavelength geoid signal can be explained with a model based on flow driven by seismically derived mantle density. The geoid together with other geophysical processes (post-glacier rebound (Mitrovica & Peltier, 1991; Lau et al., 2016, 2018), dynamic uplift (Kiefer & Hager, 1992), plate motions (Osei Tutu et al., 2018), etc.) have been used to constrain both the relative and absolute viscosities of the mantle.

Most inferences of Earth’s long-wavelength mantle viscosity structure rely on a spherically symmetric representation of viscosity [radial variation only] (Richards & Hager, 1988). This assumption permits a regional constrained viscosity-depth profile to be extended and applied over the entire globe. For example, authors have solved for the depth-dependent viscosity structure based on a regional waxing and waning of ice sheets in the past 20,000 years (Peltier, 1996). Such regionally constrained viscosity profiles may at best be representative of the local viscosity-depth variations beneath the glaciated area and immediate surroundings (M. Simons & Hager, 1997), and perhaps not applicable to other areas of the globe.

Here we use a new method to develop the new large-scale regional estimates of the mantle’s long-wavelength radial viscosity structure using Earth’s static geoid. These estimates illustrate how strong regional mantle heterogeneities (or lack thereof) influence the regional radial viscosity structure. We employ a spatio-spectral localization technique (Slepian basis functions – see Method and data) to study any potential differences that

61 may exist between global and regionally constrained radial viscosity structures. We use
 62 a Bayesian inversion approach to solve for local mantle viscosity profiles in two unique
 63 regions of the present-day mantle. The first region covers the circum-Pacific, encompass-
 64 ing most of the present-day active subduction systems in and around the Pacific plate
 65 (fig. 1a). The second region covers an area with predominately less active or recently ac-
 66 tive subduction zones centered in the Atlantic-Africa hemisphere. Compared to Kido et
 67 al. (1998), we demarcate the mantle into two parts considering slabs locations. Kido et
 68 al. (1998) applied genetic algorithm to infer local viscosity considering continental and
 69 oceanic mantle regions.

70 The regional viscosity inversion is used to highlight the importance of local man-
 71 tle heterogeneities, such as subduction, slabs and other regional geodynamic processes,
 72 to mantle radial viscosity characteristics. Large-scale mantle flow studies generally in-
 73 voke subducted slab structure and rheology to explain lateral viscosity variations (Ghosh
 74 et al., 2010; Zhong & Davies, 1999). There is no established relation on the plausible in-
 75 fluence of slabs rheology to the radial mantle viscosity structure. Slabs seen in seismic
 76 tomography models occupy a low volume of the overall mantle. Rigid slab remnants are
 77 mainly concentrated in the upper mantle and the uppermost lower mantle where they
 78 make up a relatively larger volume (Christensen, 1988; Fukao et al., 2001; Hayes et al.,
 79 2018). The complexity of slabs geometry with the different styles and stages of subduc-
 80 tion (Fukao et al., 2001), concentrated in specific regions and depths of the mantle (fig. 1a
 81 and Supplementary Information fig. S1b), may suggest local radial viscosity profiles that
 82 are unique to regions of the mantle. Mantle viscosity is known to be dependent on both
 83 chemical (e.g., major mineral assemblage such as Ferropericlase and Bridgmanite) and
 84 physical (e.g., temperature, pressure, deformation mechanism, strain rate, grain size) prop-
 85 erties.

86 2 Method and data

87 We focus on regional constraints of Earth’s 1D viscosity structure in two tectonic
 88 regimes, using a convective geoid model based on seismic and slab density models. We
 89 analyzed the geoid data in the spectral ranges $l = 2$ to 3 (long-wavelengths) and $l =$
 90 4 to 9 (intermediate wavelengths). The intermediate range (i.e. $l = 4-9$) of the geoid
 91 has been shown to be more sensitive to density variations due to subducted slabs (Hager,
 92 1984), whereas the long wavelength geoid ($l = 2-3$) is sensitivity to lower mantle den-
 93 sity structure.

94 We use local geoid kernels based on Slepian basis functions (Wieczorek & Simons,
 95 2005) for the regional viscosity inversions. In most regional geophysical data analysis based
 96 on global data, one of the important issues that often needs further consideration is spec-
 97 tral leakage and/or contamination of the data signal in the region of interest (Wieczorek
 98 & Simons, 2005). In our case, it is very important to understand the extent of depth con-
 99 tributions from the local mantle heterogeneities, and explicitly seek to minimize any leak-
 100 ages with respect to depth and lateral influences. For example, considering an iso-viscous
 101 mantle, we can test the local sensitivity kernels ($L=1-30$ in FigS. 1e and $L = 1-9$ in Fig.1b
 102 main text) for sensitivity to a sub-surface anomaly in a location of the mantle to show
 103 the robustness of our method at depth and lateral extent for different bandwidths.

104 Local and global geoid kernels: Forward modeling

105 We constrain local mantle viscosity and density structure for two unique regions
 106 (i.e., Pacific and Atlantic hemispheres) using a Bayesian probabilistic inversion with lo-
 107 cal non-hydrostatic geoid data. We analyze the geoid data in the spectral ranges $l =$
 108 2 to 3 and $l = 4$ to 9.

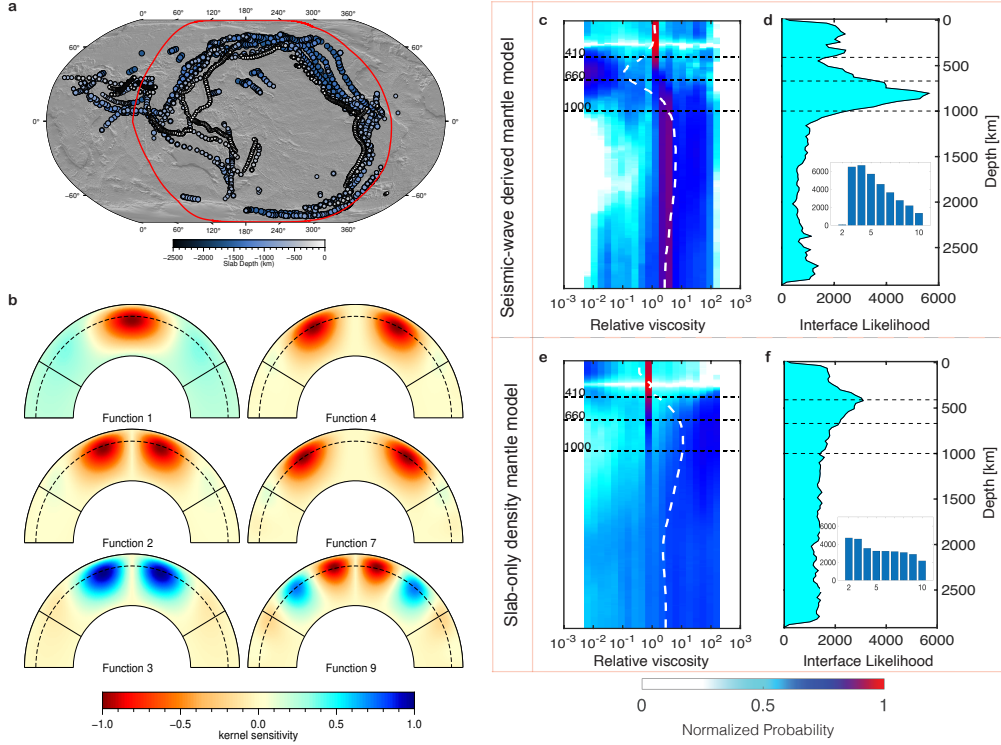


Figure 1. a) An outline (red line) of our Pacific region for the local constrain layered mantle viscosity inversions showing locations and depths of present-day slabs distribution (Lithgow-Bertelloni & Richards, 1998) in the mantle. b) Local sensitivity dynamic geoid kernels with an iso-viscous mantle. Shown is a cross-section along 0° and 180° in the northern hemisphere from the surface to the core mantle boundary. The kernels have azimuthal dependence and as such will have different manifestations at different azimuths. The kernels are localized to a 50° spherical cap, denoted by black lines connecting the surface to the core mantle boundary and the dash lines show the 670 km depth. The bandwidth of the basis is $l = 9$. Functions are ranked by concentration within the region, and shown are functions 1, 2, 3, 4, 7, and 9. Here the kernels are normalized by their maximum absolute value. The kernels can be localized in both regular and irregular (red outline) spherical caps. c) Layered mantle viscosity solutions from global large-scale mantle flow for spherical harmonics degrees $l = 2$ to 3 using a seismically-derived mantle model (French & Romanowicz, 2015) (c-d) with constant scaling and plate reconstruction slab-only mantle model (Steinberger, 2000) (e-f). Panels c and e show 2D histograms of the posterior probability distributions of viscosity with depths expressed as normalized probability and the white dash lines giving the mean relative viscosity profiles. Panels d and f show resulting mantle-viscosity interfaces distribution with the corresponding inset histograms giving the number of layers for each solution.

109 The spectral synthesis of regional geophysical signals from global spherical harmon-
 110 ics coefficients over a local region is often done using a localization technique such as ra-
 111 dial basis functions, wavelets (Schmidt et al., 2007), or point masses (Baur & Sneeuw,
 112 2011). Here we use Slepian basis functions (Wieczorek & Simons, 2005) to examine the
 113 local geoid in our regions. A number of previous studies have employed Slepian local-
 114 ization analysis, for example, to map Greenland Ice mass balance (e.g., Harig & Simons,
 115 2012; Bevis et al., 2019) or to study earthquake gravitational changes from the GRACE
 116 gravity data (e.g., Han & Simons, 2008). Each Slepian basis function constitutes a lin-
 117 ear combination of the spherical harmonics on a sphere, with the specific combination
 118 determined by an optimization over the local region of interest. A detailed formulation
 119 can be found in Wieczorek and Simons (2005) and F. J. Simons et al. (2006) with a prac-
 120 tical treatment presented in F. J. Simons (2010).

121 Our localization procedure combines Slepian basis functions with the non-linear
 122 Green’s response functions (known as geoid kernels) $\mathcal{G}^l(r, \eta(r))$ representing the dynamic
 123 contribution of Earth’s mantle to the anomalous geoid at the surface. The global dynamic
 124 geoid anomaly is calculated as

$$125 \quad \delta V_{lm}(\mathbf{S}) = \frac{4\pi G S}{2l+1} \int_c^S \mathcal{G}^l(r, \eta(r)) \delta \rho_{lm}(r) dr \quad (1)$$

126 where G is the gravitational constant, and l and m are the spherical harmonic degree
 127 and order respectively. r denotes the mantle radius between the surface (S) and the core
 128 mantle boundary (c). We perform a Bayesian inversion (see Supplementary Information)
 129 during which each Markov-chain Monte Carlo (MCMC) step, the proposed relative vis-
 130 cosity structure η is used to derive the geoid response function, which is convolved with
 131 the mantle lateral density heterogeneities $\delta \rho_{lm}(r)$ in spherical harmonics to synthesize
 132 the global geoid anomaly signal in spectral domain ($\delta V_{lm}(\mathbf{R})$).

133 To build our Slepian basis (and examine the local geoid signal) we use the outline
 134 of the local region of interest R , for example the red outlines in fig. 1a for our Pacific
 135 region (see Supplementary Information Fig. S2 and Fig. S3 for Pacific and Atlantic re-
 136 gions) to integrate the products of the spherical harmonics $Y_{lm}(r)$ as

$$137 \quad \int_R Y_{lm} Y_{l'm'} d\Omega = D_{lm, l'm'}. \quad (2)$$

138 The ‘localization kernel’ \mathbf{D} is then decomposed in a matrix eigenvalue equation,

$$139 \quad \sum_{l'=0}^L \sum_{m'=-l'}^{l'} D_{lm, l'm'} g_{l'm'} = \lambda g_{lm}, \quad (3)$$

140 where the Slepian basis functions g_{lm} are the eigenfunctions, and the eigenvalues $0 \leq$
 141 $\lambda \leq 1$ represent the degree of concentration of each function within the region (F. J. Si-
 142 mons et al., 2006). We show sets of sensitivity maps of the Slepian basis functions of well-
 143 concentrated functions for the Pacific (Fig. S2) and Atlantic (Fig. S2) hemispheres with
 144 $\lambda \geq 0.5$. We have applied our Slepian localization technique in a joint inversion anal-
 145 ysis of postglacial rebound and convection data to study the western shallow and east-
 146 ern cratonic upper mantle viscosity structures of North America continental area (?, ?).

147 We use the PREM (Dziewonski & Anderson, 1981) model as our depth-dependent
 148 reference density of the mantle with the geoid kernel estimation and neglect mantle com-
 149 positional variations so not to interfere with any distinct regional viscosity difference we
 150 may infer. We consider two different scenarios of the mantle structure. We first derive
 151 the mantle density structures from two seismic tomography models [SEMUCB-WM1 (French
 152 & Romanowicz, 2015) and S362ANI+M (P. Moulik, 2014)] following the relation $\delta \rho =$
 153 $\frac{\partial \ln \rho}{\partial \ln V_s}$. We test both single parameter (0.35) and depth-dependent seismic velocity-density

154 scalings (Simmons et al., 2010). We remove density heterogeneities in the top 300 km
 155 in oceans and continents due to the complex and compositional origin of continental roots.
 156 Our second mantle model scenario employs geodynamically derived slab density model
 157 STB00 (Steinberger, 2000), which is based on a tectonic plate reconstruction. Employ-
 158 ing a wide range of mantle density models will ensure that our resulting local and global
 159 viscosity-depth characteristics are not data dependent or artificial. Forte and Peltier
 160 Forte and Peltier (1991) showed the implications on the choice of mantle density structure for
 161 large-scale mantle flow viscosity inferences. They concluded that the choice of mantle
 162 internal density structure used to infer the radial mantle viscosity structure plays a ma-
 163 jor role in the resulting viscosity structure due to the sensitive nature of the viscosity
 164 profile to the mantle density model. This makes it appropriate to test different density
 165 models and also to take advantage of the recent seismic tomography with improved de-
 166 tail and resolution.

167 **3 Results and Discussion**

168 **Global constrained radial viscosity solution**

169 To better quantify the significance of regional mantle heterogeneities to radial vis-
 170 cosity, we first infer a series of global constrained viscosity profiles and verify our solu-
 171 tions with recent published studies (Rudolph et al., 2015). In each case we use a prob-
 172 abilistic sampling solution method (see Materials and Methods) to synthesize the global
 173 geoid fields and compare with the respective observed time-invariant geoid signal from
 174 GRACE (Reigber et al., 2005) satellite data to infer the global viscosity structure. We
 175 focus on long ($l = 2$ to 3) and intermediate ($l = 4$ to 9) spherical harmonic wavelengths
 176 of the geoid. The posterior distribution of our $l = 2$ to 3 globally constrained relative
 177 viscosity solution (fig. 1c) based on seismically derived mantle structure predicts a low-
 178 viscosity transition zone with strong upper mantle (i.e. above 410 km) and lower-mantle
 179 viscosities. There is roughly a one order of magnitude viscosity increase between the tran-
 180 sition zone and the lower mantle. The viscosity increase between 670 km and the lower
 181 mantle is supported by a high probability mantle interface (fig. 1d). Our globally con-
 182 strained long-wavelength ($l = 2$ to 3) viscosity structures, using seismically derived den-
 183 sity models, are consistent with past large-scale mantle flow studies (Forte et al., 1994;
 184 Steinberger & Calderwood, 2006; Rudolph et al., 2015). The $l = 2$ -3 viscosity inversion
 185 experiments with other seismic tomography models using either single parameter (Sup-
 186 plementary Information fig. S5a-b) or depth-dependent (Supplementary Information fig.
 187 S5e-f) seismic velocity-to-density scaling show similar mantle viscosity-depth character-
 188 istics.

189 For our slab-only mantle density model (Steinberger, 2000), the global $l = 2$ -3 vis-
 190 cosity solution, shows a relatively strong transition zone (fig. 1e) compared to the pre-
 191 diction using the seismic-derived mantle model (e.g., fig. 1c). Note that for the slab-only
 192 mantle, we are assuming a mantle convection style which depends on only subduction
 193 and slab material. Hence, our prediction of a strong transition zone (fig. 1e-f) is not sur-
 194 prising in the absence of hot buoyant mantle material. The large accumulation of rigid
 195 slab material within the transition zone and above 1000 km depth (Fukao et al., 2001)
 196 may be a contributing factor generating a stiff viscosity interface. This may also sug-
 197 gest a non-negligible long wavelength component of slabs' influence on viscosity-depth
 198 variations.

199 The set of intermediate wavelengths ($l = 4$ to 9) globally constrained viscosity pro-
 200 files, shows predominately the sensitivity of geoid data to slab remnants (Hager, 1984).
 201 Both the seismic-wave derived model and the slab-only mantle density models (Supple-
 202 mentary Information fig. S4a-b and S4c-d) predict a weak asthenosphere channel, fol-
 203 lowed by a stiff transition zone. Panasyuk and Hager et al. (Panasyuk & Hager, 2000)
 204 have suggested a similar layered mantle viscosity structure showing a strong transition

205 zone, using a combination of slab densities in the upper mantle and seismic-based den-
 206 sities for the lower mantle. Our results show a high probability viscosity-and-mantle in-
 207 terface around the 410-km depth with a viscosity jump of more than 2 orders of mag-
 208 nitude between the asthenosphere (upper mantle) and the mid-mantle. Such values of
 209 relative viscosity (*ca.* 300) (Hager & Richards, 1989) between the asthenosphere and lower
 210 mantle is required to fit the observed slab geoid ($l = 4$ to 9).

211 **Local constrained radial viscosity solution**

212 Using a Slepian localization technique (fig. 1b & fig. S2-S3), we derive local geoid
 213 signals (i.e. Pacific and Atlantic hemispheres) and infer a viscosity solution for each re-
 214 gion. In each case, we consider the same mantle density models and geoid spectrums (i.e.
 215 $l = 2$ to 3 and $l = 4$ to 9) used in the global solutions above. The resulting regional
 216 viscosity structures show distinct differences in the top 800 km of the mantle, particu-
 217 larly across the mantle transition zone. By comparing the $l = 2 - 3$ inferred viscosity
 218 structures for the Pacific (fig. 2a-b and 2e-f) to the Atlantic (fig. 2c-d and 2g-h) regions,
 219 we see the unique influence of the respective local mantle structures.

220 In the Pacific domain, we find some degree of stiffness in the vicinity of the tran-
 221 sition zone (fig. 2a-b and 2e-f). Conversely the Atlantic regional solutions, which have
 222 little/no-slab heterogeneities within the top 800 km of mantle, show no such stiff viscos-
 223 ity interface. Rather we infer a relatively low-viscosity transition zone (fig. 2c-d and 2g-
 224 h). A similar phenomenon is also observed for the $l = 4 - 9$ regional viscosity inversions
 225 shown in fig. 3b for the Pacific (blue lines) and Atlantic (red lines) hemispheres (see also
 226 supplementary information fig. S7). Maps showing the respective local geoid anomalies
 227 of the Pacific and Atlantic regions for $l = 2 - 3$ and $l = 4 - 9$ are provided in the sup-
 228 plementary information (fig. S9). We employed a second seismic model S362ANI+M (P. Moulik,
 229 2014) and repeat our regional calculations (fig. 3, solid lines), which show similar results
 230 for the Pacific and Atlantic local inversions (supplementary information fig. S8).

231 Localizing around and away from the subduction systems (e.g., Red outline fig. 1a)
 232 shows the apparent effect of the local mantle structures. The presences of slab hetero-
 233 geneities within the Pacific local mantle may be the controlling factor giving rise to the
 234 stiff transition zone at long (fig. 3a, green region) and intermediate wavelengths local vis-
 235 cosity solutions (fig. 3, green region). While phase changes and mantle composition pre-
 236 dominantly have been proposed to dictate the characteristics of the transition zone vis-
 237 cosity (S.-i. Karato, 2008), our results suggest additional crucial contributions from the
 238 local thermal/density structures.

239 Our understanding and interpretations of the mantle radial viscosity structure are
 240 mostly centered on the rheological properties of the global ambient mantle. The new ap-
 241 proach used here allows us to explore the potential influence of regional mantle densi-
 242 ties/temperatures to viscosity-depth variations, which may be a challenge in large-scale
 243 mantle flow studies. The prediction of stiff (Pacific, fig. 3a-b [blue profiles]) and weak
 244 (Atlantic, fig. 3a-b [red profiles]) transition zone viscosities, are at first-order due to the
 245 presence and absence of slab remnants within each local mantle. This finding illuminate
 246 past conclusions (e.g. Forte et al., 1994; King, 1995; Steinberger & Calderwood, 2006;
 247 Liu & Zhong, 2016) on mantle transition zone viscosity profiles, which relied on the man-
 248 tle hot anomalies. The coupled hot mantle and cold slabs with phase transitions may
 249 be playing an equal role on the exact amplitude of the transition zone rheology. We would
 250 expect to predict similar viscosity profiles for the two regions per our assumption of spher-
 251 ical symmetry of global constrained viscosity profiles. Recently, Mao and Zhong (2021)
 252 used plate motion history in a mantle convection model to show how the strength slabs
 253 with respect to the surrounding mantle influence the modeled geoid anomalies and ob-
 254 servation. Our inferred viscosity-depth differences suggest that slab rheology may be as

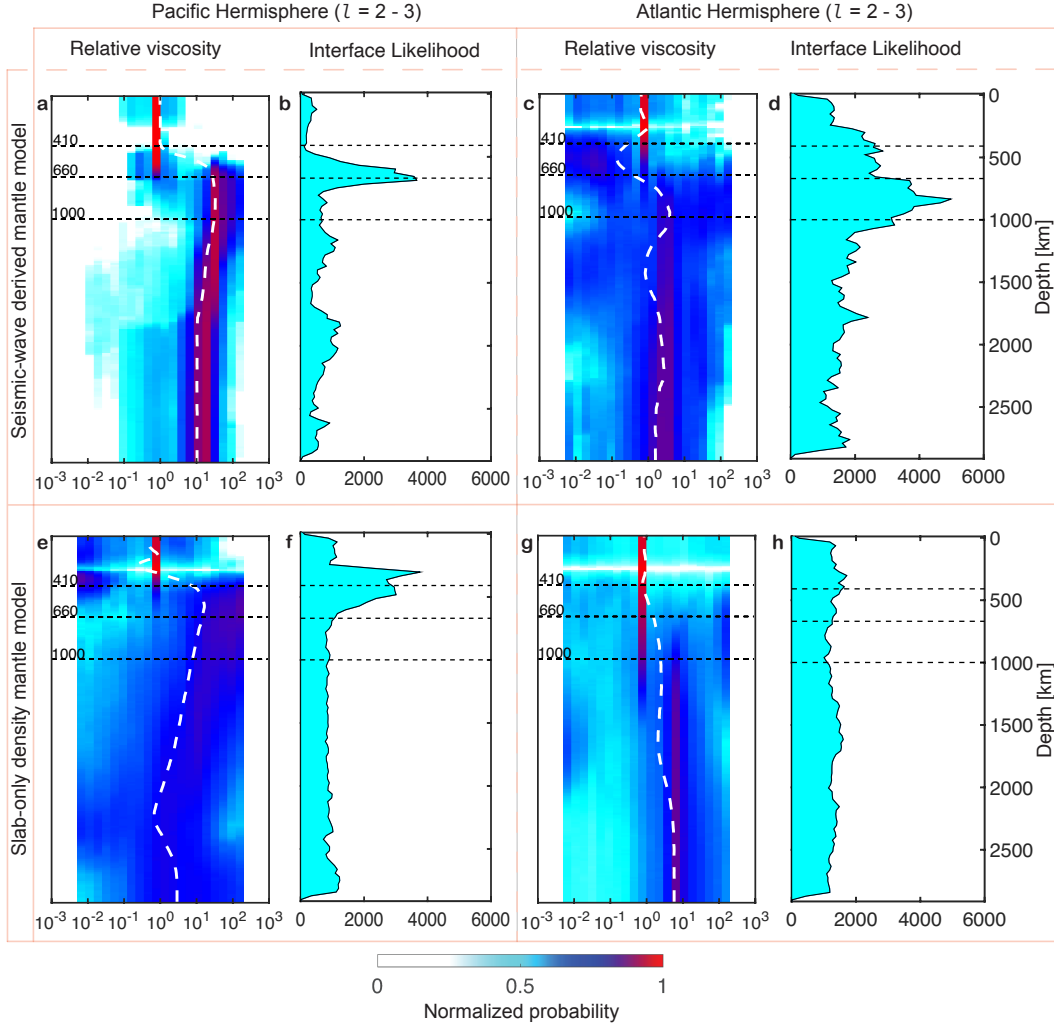


Figure 2. Long-wavelength ($l = 2 - 3$) local viscosity solutions based on regional mantle models from (a-d) seismically-derived mantle model (French & Romanowicz, 2015) and (e-h) plate reconstruction slab-only mantle model (Steinberger, 2000). Plots a, c, e, and g show 2D histograms of the posterior probability distributions of viscosity with depth, expressed as normalized probability. The white dash lines give the mean relative viscosity profiles. Panels b, d, f, and h show the resulting mantle-viscosity interfaces distributions. The left and right halves of the figure represent the inversion solutions for spherical harmonics degrees $l = 2 - 3$ for the Pacific and Atlantic regions, respectively.

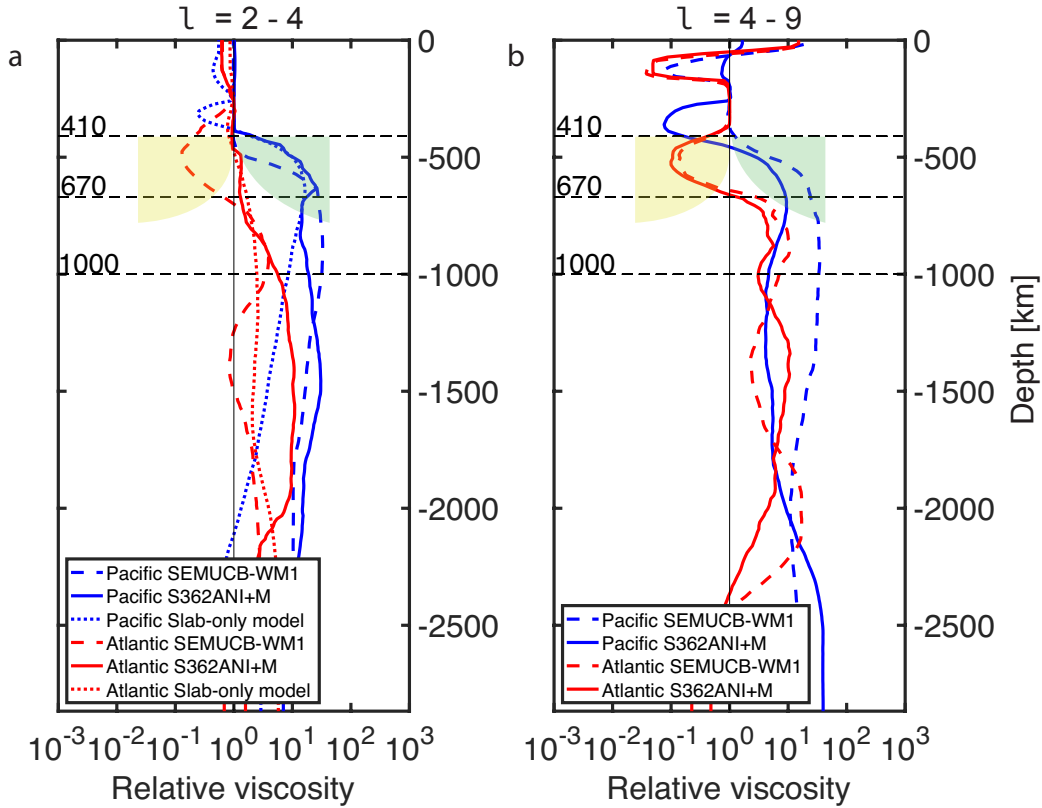


Figure 3. Plots showing a) the averages of long-wavelength ($l = 2 - 3$) local viscosity solutions based on seismically-derived mantle model SECUMB-WM1 (French & Romanowicz, 2015) (dashed), *S362ANI+M* (P. Moulik, 2014) (solid) and slab-only mantle model (Steinberger, 2000) (dotted) for the Pacific (blue) and Atlantic (red). b) Averages of intermediate-wavelength ($l = 4 - 9$) local viscosity solutions based on seismically-derived mantle model SECUMB-WM1 (French & Romanowicz, 2015) (dashed), *S362ANI+M* (P. Moulik, 2014) (solid) for the Pacific (blue) and Atlantic (red). The yellow and green shaded regions show the respective Atlantic and Pacific viscosity solutions interface preference in the top mantle.

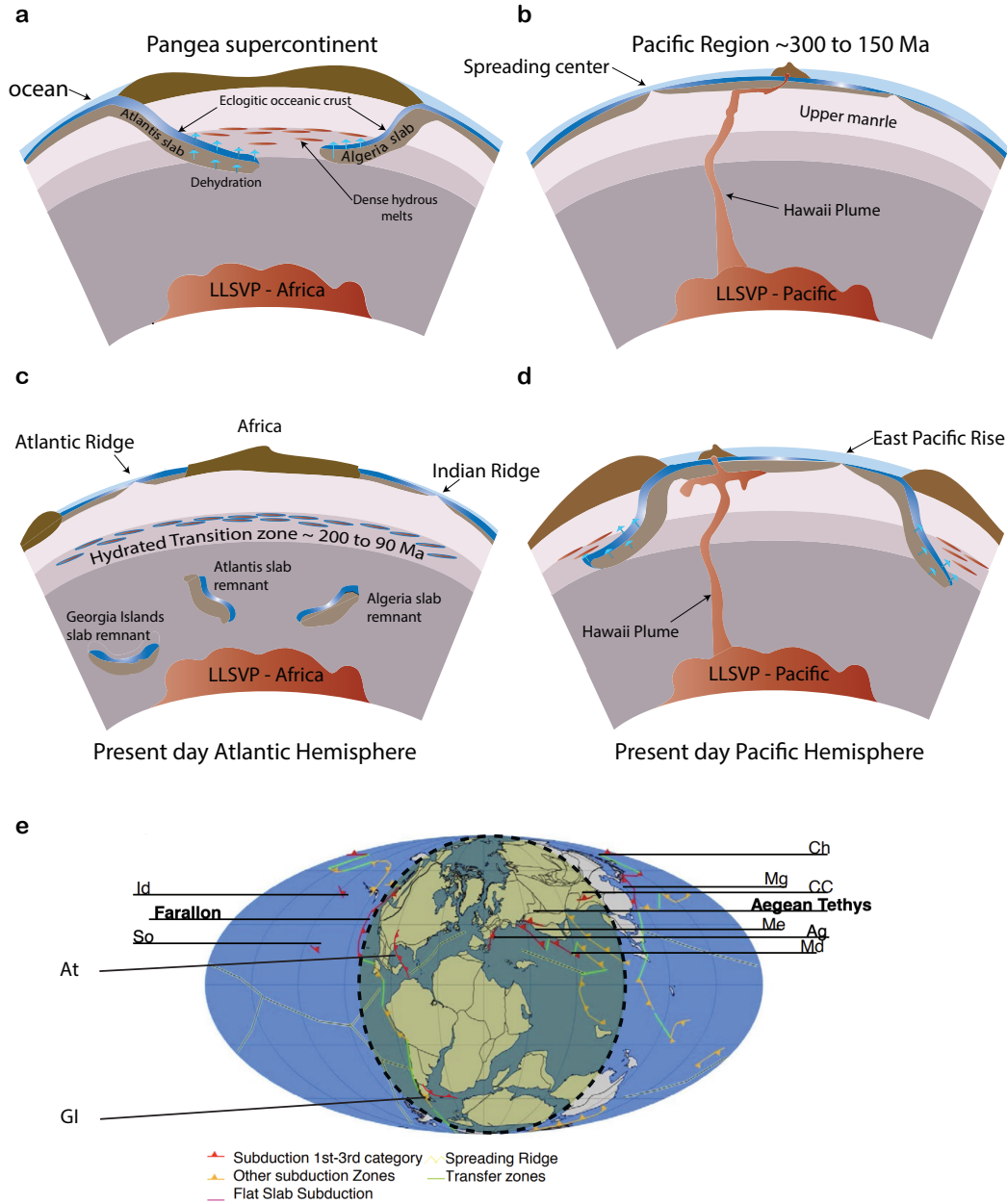


Figure 4. Schematic illustration of a possible hemispheric difference between (a) Atlantic and (b) Pacific regions during the Jurassic and Early Cretaceous eras showing the peripheral subduction of the Pangea supercontinent and spreading centers respectively. (c) Present-day Atlantic hemisphere showing a possible hydrated transition zone and/or top of the lower mantle from past subduction with remnants of the Atlantis, Algeria and Georgia Island slabs in the deep mantle. (d) Pacific region showing present-day subduction systems and the Hawaii plume. (e) A Paleo-Geographic map with the longitudinal position of past oceanic subduction zones modified after van der Meer et al., (van der Meer et al., 2010) depicting the likely position of the Ag – Algeria, CC – Central China, Ch – Chukchi, Id – Idaho, Me – Mesopotamia, At – Atlantis, Mg – Mongolia, GI Georgia Islands, So – Socorro, Md – Maldives slabs. The overlying yellow shade with dash black outline shows the approximate Atlantic region for the local viscosity inversion with our spatio-spectral localization technique.

255 important to the layered mantle viscosity as it is to lateral viscosity variations, especially
256 in the top 800-km of the mantle.

257 Subducted oceanic crust in the mantle transition zone contains garnet-rich layers
258 (Majorite). These layers have been suggested (S.-I. Karato et al., 1995) as a major con-
259 tributing factor for the strong transition zone viscosity. The prediction of low-viscosity
260 interfaces with our less/no slabs region (fig. 3 [red]) versus the stiffness obtained with
261 the slabs dominated Pacific local mantle (fig. 3 [blue]) tends to support this observation.
262 The presence of other garnet-rich composition within the mantle transition zone in the
263 form of either pyrolite or piclogite (i.e. peridotite and eclogite) will also influence the Pa-
264 cific and Atlantic local viscosity profiles. But the high volumetric ratio [about 90% (S.-
265 I. Karato et al., 1995)] of garnet constituents in subducted oceanic crust and cold slabs
266 structures within our Pacific region of the mantle will likely account for most of the ex-
267 tra hardness within the transition zone. The debate surrounding stiff (Ricard et al., 1989;
268 King, 1995) or weak transition zone (Forte et al., 2013) dates back several decades among
269 large-scale mantle flow studies. This discrepancy may be due to the intrinsic deficien-
270 cies among the global seismic models used for those studies, since slabs are resolved dif-
271 ferently in various seismic models. Our viscosity localization experiments may shed light
272 on the debate of the origins of hard and soft transition zone viscosity.

273 Our inference of Atlantic region low viscosity interface may have additional influ-
274 ence of a wet transition zone and the top of the lower mantle by slabs dehydration (Ohtani
275 et al., 2018) from the Pangea subduction system. The presence of water in the upper
276 mantle has been shown to affect viscosity and as a source of melting generation (S.-I. Karato
277 et al., 1995). Ohtani et al. (2018) recently showed as slabs descends into the mantle they
278 hydrate the mantle layers above (fig. 4). Their experiment suggest that dense hydrous
279 magma may form at the base of the upper mantle and move upward as slabs dehydrate.
280 As cold hydrated slabs pass the transition zone into the lower mantle either by mantle
281 suction or gravitational collapse fluids/volatile-rich magmas may generate due to the wide
282 variation in water content between mineral composition of the mantle transition zone
283 and the lower mantle. Though this phenomenon is mostly likely to be observed in the
284 Pacific region with the present-day subduction. Paleo-subduction studies (e.g., van der
285 Meer et al., 2010) constraining longitudinal positions of past oceanic subduction zones
286 showed the Atlantic mantle has experienced a period of active subduction comparable
287 to the present-day Pacific subduction systems. van der Meer et al. (2010) mapped out
288 the current locations of slab remnants in the mid and lower mantle using plate recon-
289 struction and seismic model (supplementary information fig. S11). Their analysis showed
290 that most lower mantle slabs materials are concentrated in the Atlantic region, for ex-
291 ample the Atlantis, Georgia Island, Algeria, Farallon plates, etc (fig. 4a). It's possible
292 such volatile-rich mantle depths induced by past Pangea subduction may persist over
293 100 - 200 Myr (fig. 4c), which will affect our Atlantic viscosity inference.

294 A number of authors have suggested the presence/remnants of distinct heating (or
295 temperatures) within the respective local mantles (Lenardic et al., 2011; Le Pichon et
296 al., 2019; Karlsen et al., 2021) considered in our current study. According to Le Pichon
297 et al. (2019), the assemblage and stationarity of the supercontinent Pangea with periph-
298 eral subduction systems led to a thermally insulated mantle. A recent study by Karlsen
299 et al. (2021) of the two hemispheres (Pacific and Atlantic), has suggested a temperature
300 deficit of about 50K with the Pacific region been colder, which will in turn make the Pa-
301 cific mantle relatively stronger. We explore this by localizing in central Pacific exclud-
302 ing all slab to infer viscosity and compared with inversion focusing on western Pacific
303 (see supplementary information Fig. S10). The central Pacific mantle gave a less stiff
304 upper mantle compared to the western Pacific region with old slabs suggestion this tem-
305 perature deficit may have less influence on our results compared to subducted oceanic
306 plate.

307 4 Conclusion

308 In summary, we suggest that regional mantle structures have a unique control on
309 the local viscosity inference and likely the global viscosity profile. Especially within the
310 top 800 km of the mantle, slabs heterogeneities show non-negligible influence on the viscosity-
311 depths variations in the mantle transition zone. There may be additional contributions
312 from a difference in the regional mantle hydrations. Our findings put a first-order con-
313 straint on the long-wavelength lateral viscosity variations within the top half of the man-
314 tle. This is characterized by the presence of a strong transition zone in and around pre-
315 dominantly slabs and subducting regions, combined with a comparatively low-viscosity
316 transition zone. The inferred significance of slab rheology to the depth-dependent vis-
317 cosity structure suggests global profiles created with the assumption of spherically sym-
318 metric mantle flow driven only by ambient density should be interpreted cautiously in
319 regional settings, even at large scales.

320 5 Open Research

321 Figures were created with GMT and Matlab. The model output and code used for
322 our calculations will be made available at Zenodo ([http://doi.org/10.5281/zenodo](http://doi.org/10.5281/zenodo.6585021)
323 [.6585021](http://doi.org/10.5281/zenodo.6585021)) (Osei Tutu et al., 2022) .

324 Acknowledgments

325 We thank the University of Arizona’s High Performance Computing center for granting
326 us the free computational resources used for this study. We thank Bernhard Steinberger,
327 Vedran Lekić and Raj Moulik for helpful discussions, and Shijie Zhong who read an early
328 version of this manuscript. **Funding:** This work was made possible by NASA grant NNX17AE18G
329 to CH.

330

References

331

Baur, O., & Sneeuw, N. (2011, Sep 01). Assessing greenland ice mass loss by means of point-mass modeling: a viable methodology. *Journal of Geodesy*, *85*(9), 607–615. Retrieved from <https://doi.org/10.1007/s00190-011-0463-1> doi: 10.1007/s00190-011-0463-1

332

333

334

Bevis, M., Harig, C., Khan, S. A., Brown, A., Simons, F. J., Willis, M., . . . Nylén, T. (2019). Accelerating changes in ice mass within greenland, and the ice sheet's sensitivity to atmospheric forcing. *Proceedings of the National Academy of Sciences*, *116*(6), 1934–1939. Retrieved from <https://www.pnas.org/content/116/6/1934> doi: 10.1073/pnas.1806562116

335

336

337

338

339

Christensen, U. (1988). Is subducted lithosphere trapped at the 670-km discontinuity? *Nature*, *336*(6198), 462–463. Retrieved from <https://doi.org/10.1038/336462a0> doi: 10.1038/336462a0

340

341

342

Dziewonski, A. M., & Anderson, D. L. (1981). Preliminary reference earth model. *Physics of the Earth and Planetary Interiors*, *25*(4), 297–356. doi: [https://doi.org/10.1016/0031-9201\(81\)90046-7](https://doi.org/10.1016/0031-9201(81)90046-7)

343

344

345

Forte, A. M., Dziewonski, A. M., & Woodward, R. L. (2013). A spherical structure of the mantle, tectonic plate motions, nonhydrostatic geoid, and topography of the core-mantle boundary. In *Dynamics of earth's deep interior and earth rotation* (p. 135-166). American Geophysical Union. Retrieved from <https://agupubs.onlinelibrary.wiley.com/doi/abs/10.1029/GM072p0135> doi: 10.1029/GM072p0135

346

347

348

349

350

351

Forte, A. M., & Peltier, R. (1991). Viscous flow models of global geophysical observables: 1. forward problems. *Journal of Geophysical Research: Solid Earth*, *96*(B12), 20131-20159. Retrieved from <https://agupubs.onlinelibrary.wiley.com/doi/abs/10.1029/91JB01709> doi: 10.1029/91JB01709

352

353

354

355

Forte, A. M., Woodward, R. L., & Dziewonski, A. M. (1994). Joint inversions of seismic and geodynamic data for models of three-dimensional mantle heterogeneity. *Journal of Geophysical Research: Solid Earth*, *99*(B11), 21857-21877. Retrieved from <https://agupubs.onlinelibrary.wiley.com/doi/abs/10.1029/94JB01467> doi: 10.1029/94JB01467

356

357

358

359

360

French, S., & Romanowicz, B. (2015). Broad plumes rooted at the base of the earth's mantle beneath major hotspots. *Nature*, *525*, 95. Retrieved from <https://www.nature.com/articles/nature14876supplementary-information> doi: <https://doi.org/10.1038/nature14876>

361

362

363

364

Fukao, Y., Widiyantoro, S., & Obayashi, M. (2001). Stagnant slabs in the upper and lower mantle transition region. *Reviews of Geophysics*, *39*(3), 291-323. Retrieved from <https://agupubs.onlinelibrary.wiley.com/doi/abs/10.1029/1999RG000068> doi: 10.1029/1999RG000068

365

366

367

368

Ghosh, A., Becker, T. W., & Zhong, S. J. (2010). Effects of lateral viscosity variations on the geoid. *Geophysical Research Letters*, *37*(1). Retrieved from <https://agupubs.onlinelibrary.wiley.com/doi/abs/10.1029/2009GL040426> doi: 10.1029/2009GL040426

369

370

371

372

Hager, B. H. (1984). Subducted slabs and the geoid: Constraints on mantle rheology and flow. *Journal of Geophysical Research: Solid Earth*, *89*(B7), 6003-6015. Retrieved from <https://agupubs.onlinelibrary.wiley.com/doi/abs/10.1029/JB089iB07p06003> doi: 10.1029/JB089iB07p06003

373

374

375

376

Hager, B. H., & Richards, M. A. (1989). Long-wavelength variations in earth's geoid: Physical models and dynamical implications. *Philosophical Transactions of the Royal Society of London. Series A, Mathematical and Physical Sciences*, *328*(1599), 309–327.

377

378

379

380

Han, S.-C., & Simons, F. J. (2008). Spatiospectral localization of global geopotential fields from the gravity recovery and climate experiment (grace) reveals the co-seismic gravity change owing to the 2004 sumatra-andaman earthquake. *Journal of Geophysical Research: Solid Earth*, *113*(B1). Retrieved from <https://>

381

382

383

384

- 385 agupubs.onlinelibrary.wiley.com/doi/abs/10.1029/2007JB004927 doi:
386 10.1029/2007JB004927
- 387 Harig, C., & Simons, F. J. (2012). Mapping greenland's mass loss in space and time.
388 *Proceedings of the National Academy of Sciences*, 109(49), 19934–19937. Re-
389 trieved from <https://www.pnas.org/content/109/49/19934> doi: 10.1073/
390 pnas.1206785109
- 391 Hayes, G. P., Moore, G. L., Portner, D. E., Hearne, M., Flamme, H., Furt-
392 ney, M., & Smoczyk, G. M. (2018). Slab2, a comprehensive subduc-
393 tion zone geometry model. *Science*, 362(6410), 58–61. Retrieved from
394 <https://science.sciencemag.org/content/362/6410/58> doi: 10.1126/
395 science.aat4723
- 396 Karato, S.-i. (2008). *Deformation of earth materials: An introduction to the rheology*
397 *of solid earth*. Cambridge University Press. doi: 10.1017/CBO9780511804892
- 398 Karato, S.-I., Wang, Z., Liu, B., & Fujino, K. (1995). Plastic deformation of gar-
399 nets: systematics and implications for the rheology of the mantle transition
400 zone. *Earth and Planetary Science Letters*, 130(1), 13 - 30. Retrieved from
401 <http://www.sciencedirect.com/science/article/pii/0012821X9400255W>
402 doi: [https://doi.org/10.1016/0012-821X\(94\)00255-W](https://doi.org/10.1016/0012-821X(94)00255-W)
- 403 Karlsen, K. S., Conrad, C. P., Domeier, M., & Trønnes, R. G. (2021). Spa-
404 tiotemporal variations in surface heat loss imply a heterogeneous mantle
405 cooling history. *Geophysical Research Letters*, 48(6), e2020GL092119. doi:
406 <https://doi.org/10.1029/2020GL092119>
- 407 Kido, M., Yuen, D. A., Čadek, O., & Nakakuki, T. (1998). Mantle viscosity derived
408 by genetic algorithm using oceanic geoid and seismic tomography for whole-
409 mantle versus blocked-flow situations. *Physics of the Earth and Planetary Inte-*
410 *riors*, 107(4), 307-326. doi: [https://doi.org/10.1016/S0031-9201\(98\)00077-6](https://doi.org/10.1016/S0031-9201(98)00077-6)
- 411 Kiefer, W. S., & Hager, B. H. (1992, 01). Geoid anomalies and dynamic topography
412 from convection in cylindrical geometry: applications to mantle plumes on
413 Earth and Venus. *Geophysical Journal International*, 108(1), 198-214. Re-
414 trieved from <https://doi.org/10.1111/j.1365-246X.1992.tb00850.x> doi:
415 10.1111/j.1365-246X.1992.tb00850.x
- 416 King, S. D. (1995, 12). Radial models of mantle viscosity: results from a genetic
417 algorithm. *Geophysical Journal International*, 122(3), 725-734. Retrieved
418 from <https://doi.org/10.1111/j.1365-246X.1995.tb06831.x> doi:
419 10.1111/j.1365-246X.1995.tb06831.x
- 420 Lau, H. C. P., Austermann, J., Mitrovica, J. X., Crawford, O., Al-Attar, D., & Laty-
421 chev, K. (2018). Inferences of mantle viscosity based on ice age data sets: The
422 bias in radial viscosity profiles due to the neglect of laterally heterogeneous
423 viscosity structure. *Journal of Geophysical Research: Solid Earth*, 123(9),
424 7237-7252. doi: <https://doi.org/10.1029/2018JB015740>
- 425 Lau, H. C. P., Mitrovica, J. X., Austermann, J., Crawford, O., Al-Attar, D., & Laty-
426 chev, K. (2016). Inferences of mantle viscosity based on ice age data sets:
427 Radial structure. *Journal of Geophysical Research: Solid Earth*, 121(10),
428 6991-7012. doi: <https://doi.org/10.1002/2016JB013043>
- 429 Lenardic, A., Moresi, L., Jellinek, A. M., O'Neill, C. J., Cooper, C. M., & Lee, C. T.
430 (2011). Continents, supercontinents, mantle thermal mixing, and mantle ther-
431 mal isolation: Theory, numerical simulations, and laboratory experiments.
432 *Geochemistry, Geophysics, Geosystems*, 12(10). Retrieved from [https://](https://agupubs.onlinelibrary.wiley.com/doi/abs/10.1029/2011GC003663)
433 agupubs.onlinelibrary.wiley.com/doi/abs/10.1029/2011GC003663 doi:
434 10.1029/2011GC003663
- 435 Le Pichon, X., Şengör, A. M. C., & İmren, C. (2019). Pangea and the lower
436 mantle. *Tectonics*, 38(10), 3479-3504. Retrieved from [https://agupubs](https://agupubs.onlinelibrary.wiley.com/doi/abs/10.1029/2018TC005445)
437 [.onlinelibrary.wiley.com/doi/abs/10.1029/2018TC005445](https://agupubs.onlinelibrary.wiley.com/doi/abs/10.1029/2018TC005445) doi:
438 10.1029/2018TC005445
- 439 Lithgow-Bertelloni, C., & Richards, M. A. (1998). The dynamics of cenozoic and

- 440 mesozoic plate motions. *Reviews of Geophysics*, 36(1), 27-78. Retrieved from
 441 <https://agupubs.onlinelibrary.wiley.com/doi/abs/10.1029/97RG02282>
 442 doi: 10.1029/97RG02282
- 443 Liu, X., & Zhong, S. (2016). Constraining mantle viscosity structure for a ther-
 444 mochemical mantle using the geoid observation. *Geochemistry, Geophysics,*
 445 *Geosystems*, 17(3), 895-913. Retrieved from <https://agupubs.onlinelibrary>
 446 [.wiley.com/doi/abs/10.1002/2015GC006161](https://agupubs.onlinelibrary.wiley.com/doi/abs/10.1002/2015GC006161) doi: 10.1002/2015GC006161
- 447 Mao, W., & Zhong, S. (2021). Constraints on mantle viscosity from intermediate-
 448 wavelength geoid anomalies in mantle convection models with plate motion
 449 history. *Journal of Geophysical Research: Solid Earth*, 126(4), e2020JB021561.
 450 doi: <https://doi.org/10.1029/2020JB021561>
- 451 Mitrovica, J. X., & Peltier, W. R. (1991). On postglacial geoid subsidence over
 452 the equatorial oceans. *Journal of Geophysical Research: Solid Earth*, 96(B12),
 453 20053-20071. Retrieved from <https://agupubs.onlinelibrary.wiley.com/>
 454 [doi/abs/10.1029/91JB01284](https://agupubs.onlinelibrary.wiley.com/doi/abs/10.1029/91JB01284) doi: 10.1029/91JB01284
- 455 Ohtani, E., Yuan, L., Ohira, I., Shatskiy, A., & Litasov, K. (2018). Fate of water
 456 transported into the deep mantle by slab subduction. *Journal of Asian Earth*
 457 *Sciences*, 167, 2-10. doi: <https://doi.org/10.1016/j.jseas.2018.04.024>
- 458 Osei Tutu, A., Gourley, k., & Harig, C. (2022). *Variations in earth's 1d viscos-*
 459 *ity structure in different tectonic regimes.* [dataset,software]. Retrieved from
 460 <http://doi.org/10.5281/zenodo.6585021> doi: 10.5281/zenodo.6585021
- 461 Osei Tutu, A., Sobolev, S. V., Steinberger, B., Popov, A. A., & Rogozhina, I. (2018).
 462 Evaluating the influence of plate boundary friction and mantle viscosity on
 463 plate velocities. *Geochemistry, Geophysics, Geosystems*, 19(3), 642-666.
 464 Retrieved from <https://agupubs.onlinelibrary.wiley.com/doi/abs/>
 465 [10.1002/2017GC007112](https://agupubs.onlinelibrary.wiley.com/doi/abs/10.1002/2017GC007112) doi: 10.1002/2017GC007112
- 466 Panasyuk, S. V., & Hager, B. H. (2000, 12). Inversion for mantle viscosity
 467 profiles constrained by dynamic topography and the geoid, and their es-
 468 timated errors. *Geophysical Journal International*, 143(3), 821-836. Re-
 469 trieved from <https://doi.org/10.1046/j.0956-540X.2000.01286.x> doi:
 470 10.1046/j.0956-540X.2000.01286.x
- 471 Peltier, W. R. (1996). Mantle viscosity and ice-age ice sheet topography. *Science*,
 472 273(5280), 1359-1364. Retrieved from <https://science.sciencemag.org/>
 473 [content/273/5280/1359](https://science.sciencemag.org/content/273/5280/1359) doi: 10.1126/science.273.5280.1359
- 474 P. Moulik, G. E. (2014). An anisotropic shear velocity model of the earth's mantle
 475 using normal modes, body waves, surface waves and long-period waveforms.
 476 *Geophysical Journal International*, 199, 1713-1738.
- 477 Reigber, C., Schmidt, R., Flechtner, F., König, R., Meyer, U., Neumayer, K.-H.,
 478 ... Zhu, S. Y. (2005). An earth gravity field model complete to degree and
 479 order 150 from grace: Eigen-grace02s. *Journal of Geodynamics*, 39(1), 1 -
 480 10. Retrieved from [http://www.sciencedirect.com/science/article/pii/](http://www.sciencedirect.com/science/article/pii/S0264370704000754)
 481 [S0264370704000754](http://www.sciencedirect.com/science/article/pii/S0264370704000754) doi: <https://doi.org/10.1016/j.jog.2004.07.001>
- 482 Ricard, Y., Vigny, C., & Froidevaux, C. (1989). Mantle heterogeneities, geoid,
 483 and plate motion: A monte carlo inversion. *Journal of Geophysical Re-*
 484 *search: Solid Earth*, 94(B10), 13739-13754. Retrieved from <https://>
 485 agupubs.onlinelibrary.wiley.com/doi/abs/10.1029/JB094iB10p13739
 486 doi: 10.1029/JB094iB10p13739
- 487 Richards, & Hager, H. B., Richards M.A. (1988). The earth's geoid and the large-
 488 scale structure of mantle convection. , 247-272.
- 489 Richards, M. A., & Hager, B. H. (1984). Geoid anomalies in a dynamic earth. *Jour-*
 490 *nal of Geophysical Research: Solid Earth*, 89(B7), 5987-6002. Retrieved
 491 from <https://agupubs.onlinelibrary.wiley.com/doi/abs/10.1029/>
 492 [JB089iB07p05987](https://agupubs.onlinelibrary.wiley.com/doi/abs/10.1029/JB089iB07p05987) doi: 10.1029/JB089iB07p05987
- 493 Rudolph, M. L., Lekić, V., & Lithgow-Bertelloni, C. (2015). Viscosity jump
 494 in earth's mid-mantle. *Science*, 350(6266), 1349-1352. Retrieved from

- 495 <http://science.sciencemag.org/content/350/6266/1349> doi: 10.1126/
496 science.aad1929
- 497 Schmidt, M., Fengler, M., Mayer-Gürr, T., Eicker, A., Kusche, J., Sánchez, L., &
498 Han, S.-C. (2007, Jan 01). Regional gravity modeling in terms of spherical
499 base functions. *Journal of Geodesy*, 81(1), 17–38. Retrieved from [https://](https://doi.org/10.1007/s00190-006-0101-5)
500 doi.org/10.1007/s00190-006-0101-5 doi: 10.1007/s00190-006-0101-5
- 501 Simmons, N. A., Forte, A. M., Boschi, L., & Grand, S. P. (2010). Gypsum: A joint
502 tomographic model of mantle density and seismic wave speeds. *Journal of Geo-*
503 *physical Research: Solid Earth*, 115(B12). Retrieved from [https://agupubs](https://agupubs.onlinelibrary.wiley.com/doi/abs/10.1029/2010JB007631)
504 [.onlinelibrary.wiley.com/doi/abs/10.1029/2010JB007631](https://agupubs.onlinelibrary.wiley.com/doi/abs/10.1029/2010JB007631) doi: 10.1029/
505 2010JB007631
- 506 Simons, F. J. (2010). *Slepian functions and their use in signal estimation and spec-*
507 *tral analysis* (Vol. 30). doi: doi:10.1007/978-3-642-01546-5_30
- 508 Simons, F. J., Dahlen, F. A., & Wieczorek, M. A. (2006). Spatiospectral concentra-
509 tion on a sphere. *SIAM Review*, 48(3), 504–536. Retrieved from [https://doi](https://doi.org/10.1137/S0036144504445765)
510 [.org/10.1137/S0036144504445765](https://doi.org/10.1137/S0036144504445765) doi: 10.1137/S0036144504445765
- 511 Simons, M., & Hager, B. H. (1997). Localization of the gravity field and the signa-
512 ture of glacial rebound. *Nature*, 390(6659), 500–504. Retrieved from [https://](https://doi.org/10.1038/37339)
513 doi.org/10.1038/37339 doi: 10.1038/37339
- 514 Steinberger, B. (2000). Slabs in the lower mantle — results of dynamic mod-
515 elling compared with tomographic images and the geoid. *Physics of*
516 *the Earth and Planetary Interiors*, 118(3), 241 - 257. Retrieved from
517 <http://www.sciencedirect.com/science/article/pii/S0031920199001727>
518 doi: [https://doi.org/10.1016/S0031-9201\(99\)00172-7](https://doi.org/10.1016/S0031-9201(99)00172-7)
- 519 Steinberger, B., & Calderwood, A. R. (2006). Models of large-scale viscous flow
520 in the Earth’s mantle with constraints from mineral physics and surface
521 observations. *Geophysical Journal International*, 167(3), 1461–1481. Re-
522 trieved from <https://doi.org/10.1111/j.1365-246X.2006.03131.x> doi:
523 10.1111/j.1365-246X.2006.03131.x
- 524 van der Meer, D. G., Spakman, W., van Hinsbergen, D. J. J., Amaru, M. L.,
525 & Torsvik, T. H. (2010). Towards absolute plate motions constrained
526 by lower-mantle slab remnants. *Nature Geoscience*, 3(1), 36–40. doi:
527 <https://doi.org/10.1038/ngeo708>
- 528 Wieczorek, M. A., & Simons, F. J. (2005, 09). Localized spectral analysis on the
529 sphere. *Geophysical Journal International*, 162(3), 655–675. Retrieved from
530 <https://doi.org/10.1111/j.1365-246X.2005.02687.x> doi: 10.1111/j.1365-
531 -246X.2005.02687.x
- 532 Zhong, S., & Davies, G. F. (1999). Effects of plate and slab viscosities on the
533 geoid. *Earth and Planetary Science Letters*, 170(4), 487 - 496. Retrieved from
534 <http://www.sciencedirect.com/science/article/pii/S0012821X99001247>
535 doi: [https://doi.org/10.1016/S0012-821X\(99\)00124-7](https://doi.org/10.1016/S0012-821X(99)00124-7)